Materials Research Bulletin 49 (2014) 537–543

Contents lists available at ScienceDirect

Materials Research Bulletin

journal homepage: www.elsevier.com/locate/matresbu

Controlling the size and optical properties of ZnO nanoparticles by capping with SiO_2

K. Sowri Babu *, A. Ramachandra Reddy, K. Venugopal Reddy

Department of Physics, National Institute of Technology Warangal, Warangal 506 004, Andhra Pradesh, India

ARTICLE INFO

Article history:
Received 22 February 2013
Received in revised form 12 September 2013
Accepted 16 September 2013
Available online 23 September 2013

Keywords:
A. Composites
A. Nanostructures
A. Semiconductors
D. Luminescence

ABSTRACT

The size and shape of the ZnO nanoparticles synthesized through sol–gel method were controlled by capping with SiO_2. X-ray diffraction (XRD) and field emission scanning electron microscope (FE-SEM) and High Resolution Transmission Electron Microscope (HR-TEM) results demonstrated that the particle growth of the ZnO nanoparticles has been restricted to 5 nm with SiO_2 capping. As a result, the absorption spectra of ZnO nanoparticles capped with SiO_2 got blue shifted (toward lower wavelength side) due to strong quantum confinement effects. BET (Brunauer–Emmet–Teller) surface area pore size analyzer results showed that surface area of samples increased monotonously with increase of SiO_2 concentration. It was observed that the absorption spectra of ZnO capped with SiO_2 broadened with increase of SiO_2 concentration. Absorption and photoluminescence excitation results (PLE) confirmed that this broadening is due to the absorption of non-bridging oxygen hole centers (NBOHC) of SiO_2. These results also indicated that ZnO nanoparticles capped with SiO_2 are insensitive to Raman scattering. Maximum UV emission intensity was achieved with 353 nm excitation wavelength compared to 320 nm in ZnO as well as in SiO_2 capped ZnO nanoparticles. Furthermore, there is an enhancement in the intensities of emission peaks related to oxygen vacancies and interstitials with SiO_2 capping. The enhancement in the UV intensity is attributed to the surface passivation of ZnO nanoparticles and excitation processes in SiO_2.

1. Introduction

Materials exhibit novel and fascinating properties when their size is reduced to nano scale. Semiconductor nanoparticles have been widely used in optoelectronics because of their interesting size dependent optical properties. As the size of a semiconductor nanoparticle approaches the Bohr exciton radius, blue shift (shift to lower wavelength) in the absorption and emission spectra occurs. This phenomenon is called the quantum size effect. Zinc oxide (ZnO) is one of the promising II–VI semiconductors which has gained much attention due to its wide and direct band gap of 3.3 eV at 300 K and large exciton binding energy of 60 meV at room temperature [1]. Apart from these properties, ZnO is abundantly available in nature, economical and is less toxic compared to other semiconductors such as cadmium sulfide (CdS) and gallium arsenide (GaAs) [2]. Because of its distinctive properties and advantages, ZnO quantum dots (QD's) find applications in optoelectronics, sensors, cosmetics, catalysis, biomedical imaging, drug delivery and protein separation and biological fluorescence labeling [3–7]. Inspite of decades of research on luminescence of ZnO, the origin of the green luminescence is still in dispute. At first, it was assigned to the divalent copper impurities, but later on, intrinsic defects such as interstitial zinc ions or oxygen vacancies were assumed to be responsible for green emission [8–10]. Subsequent studies of Dijken et al. showed that green emission originated from a transition of an electron from a level close to the conduction band edge to a deeply trapped hole in the bulk ($V_o^{\bullet\bullet}$) of the ZnO particle [11]. Most recently, it was shown that the green luminescence originated from the hydroxyl and acetate groups attached on the surface of ZnO nanoparticles [12]. No common agreement has been reported as far as the emission properties of ZnO nanoparticles are concerned.

It is well known that optical properties of ZnO nanoparticles depend on synthesis procedures [13], defects [14], microstructure, crystallite size, orientation, morphology, lattice strain etc. [3]. However, most of the semiconductor nanoparticles exhibit size dependent optical properties. The main difficulties in ZnO QD's are uncontrollable increase in their particle size due to agglomeration and also quenching of fluorescence efficiency with aging [15]. Researchers achieved great success in surmounting these problems by encapsulating ZnO nanoparticles in SiO_2 matrix [2,15–17]. The wide use of SiO_2 as a matrix for QD's is mainly due to three advantages (i) effective control of the particle size (ii) chemical and physical inertness and (iii) its biocompatibility [15,16]. The

* Corresponding author. Tel.: +91 870 2462593; fax: +91 870 2430270.
E-mail addresses: sowribabuk@gmail.com, sowribabu@gmail.com (K.S. Babu).

0025-5408/$ – see front matter © 2013 Elsevier Ltd. All rights reserved.
http://dx.doi.org/10.1016/j.materresbull.2013.09.024

controlled particle size and stable photoluminescence have been achieved when ZnO QD's are endowed in SiO_2 matrix [16]. Moreover, the combination of ZnO with porous silicon is capable of emitting white light [18,19]. Panigrahi et al. found 2–3 nm sized ZnO QD's exhibiting negative photoconductivity when they were encapsulated in SiO_2 matrix [20]. Wu et al. witnessed the shift of the emission to visible range along with increased intensity when ZnO nanoparticles are capped with SiO_2 and TiO_2 [21]. Cao et al. demonstrated the encapsulation of Mn/Cu/Fe-doped and co-doped ZnS nanowires (NWs) and also ZnO quantum dots (QDs) with a layer of mesoporous SiO_2 [22]. Further, the authors investigated the effect of shell thickness of SiO_2 on optical properties of ZnO. Despite the advantages of easy handling and industrial use of ZnO–SiO_2 nanocomposites in powder form, the detailed studies are not available in the literature [2]. The method adopted in this study has an advantage of producing large quantities of samples in powder form.

In this work, ZnO nanoparticles were prepared by a simple sol–gel method using poly vinyl alcohol (PVA). For the preparation of SiO_2 capped ZnO nanoparticles, the as prepared ZnO nanoparticles were added to the pre-hydrolyzed SiO_2. The solution was stirred continuously during the mixing process. The particle size of the ZnO capped with SiO_2 is ten times smaller than the particle size of pristine ZnO. Consequently, absorption spectrum was seen to shift to the lower wavelength side of the spectrum. The PL spectra of the samples were measured with 320 and 353 nm excitation wavelengths. Maximum UV emission intensity was observed with 353 nm excitation wavelength in ZnO as well as in ZnO capped with SiO_2. The intensity of the UV peak and emissions related to oxygen vacancies and interstitials were enhanced with SiO_2 capping.

2. Experimental procedure

The preparation of ZnO nanoparticles using PVA is as follows: Zn $(NO_3)_2{\cdot}6H_2O$ was dissolved in a minimum quantity of de-ionized water and stirred for half an hour to obtain a homogenous cationic solution. The metal nitrate to polymer (PVA) ratio was maintained at 1:3. Required quantity of PVA was dripped slowly into de-ionized water to produce a transparent and clear solution. Subsequently, the cationic solution was mixed with PVA solution under constant stirring and heating. The stirring and heating continued until the gel like compound was formed. This gel type sample was dried at 150 °C for about 12 h in an oven to obtain ZnO nanoparticles in powder form. To prepare ZnO capped with SiO_2, one gram of the as prepared ZnO powder was added to the solution containing ethanol, distilled water, ammonia and tetraethyl orthosilicate (Sigma Aldrich; 98%) and stirred for 2 h. To study the effect of the silica content on structural and optical properties, the molarity of this solution was varied and it was 0.05 M, 0.15 M, 0.25 M and 0.5 M respectively. Later, the samples were filtered and washed with ethanol two to three times. Finally, samples were annealed in a programmable muffle furnace at 600 °C at a rate of 2 °C/min to get SiO_2 capped ZnO nanoparticles.

The structural analysis of samples was carried out by X-ray diffractometer (Bruker D8) equipped with Cu K_α radiation (λ = 1.5408 Å). The morphology, particle size and elemental analysis of the samples were probed by Field Emission-Scanning Electron Microscope (FE-SEM: model Carl Zeiss Ultra55) and JEOL 3010 HR-TEM operating at an accelerating voltage of 200 kV with Energy Dispersive Spectroscopy (EDS) attachment. Absorption spectra were acquired on Analyticazena (Specord 205) UV-vis spectrophotometer. BET analysis of the samples was carried out by Quantachrome NOVA 1200e surface area and pore size analyzer. Finally, the zeta potential of the samples was measured by Malvern Zetasizer Nano-ZS test measurement system. The influence of SiO_2 capping on ZnO vibrational bands was accomplished through IR spectroscopy, for which the samples were admixed with KBr and pelletized. The IR spectra were measured from 400 to 4000 cm^{-1} with Perkin Elmer Spectrum 100 model operating at a resolution of 4 cm^{-1}. Raman spectra of samples were recorded in the backscattering geometry at room temperature using Horiba Jobin–Yvon LabRam HR high resolution micro-Raman spectrograph with 514 nm of Argon ion laser as the excitation source. PL measurements were performed on Jobin Yuon spectrofluorometer equipped with 450 W xenon arc lamp.

3. Results and discussion

3.1. X-ray diffraction and morphological studies

X-Ray diffraction patterns of ZnO and SiO_2 capped ZnO nanoparticles prepared with different silica concentrations (0.05, 0.15, 0.25 and 0.5) are labeled as ZS1, ZS2, ZS3, ZS4 and shown in Fig. 1. The reflection peaks corresponding to the planes (100), (002), (101), (102), (110) and (103) confirmed the hexagonal wurtzite structure of ZnO nanoparticles. For the sake of clarity, only XRD patterns of pristine ZnO, ZS1, ZS3 and ZS4 are shown in the figure, because the XRD patterns of ZS2 and ZS3 appeared to be same. A broad hump was developed as the silica concentration increased and it can be clearly seen in the XRD pattern of sample ZS4. Such a hump is due to the amorphous nature of silica and it is an indication of short range ordering of silicon atoms [17]. As the silica content was increased, the broadening of peaks took place. The broadening of the diffraction peaks was caused mainly due to three reasons. They are recognized as small crystallite size, non-uniform strain and stacking faults [23]. Based on the results of FE-SEM and UV–vis spectra, discussed in the succeeding sections, the broadening of the peaks may be attributed mostly to the decrease in the crystallite size. The average crystallite size was calculated by using the Debye-Scherrer's formula for all the samples:

$$D = \frac{0.9\lambda}{\beta\cos\theta}$$

where D is the diameter of grain size (in Å), β is the FWHM of the particular peak in radians, θ is the Braggs angle and λ (0.15405 nm) is the wavelength of x-rays used. The average crystallite size values computed for ZnO, ZS1, ZS2, ZS3 and ZS4 are found to be 54 nm, 22 nm, 10 nm, 9.5 nm and 9 nm respectively. It can be seen that there is no considerable variation in the crystallite sizes of ZS2, ZS3

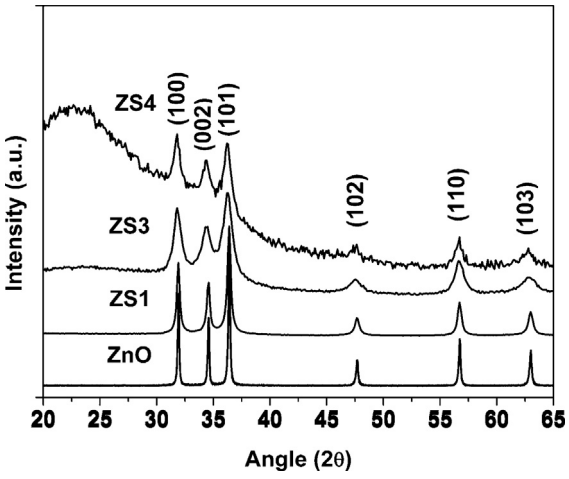

Fig. 1. X-ray diffraction patterns of ZnO nanoparticles and ZnO nanoparticles capped with different concentration of SiO_2.

and ZS4. In addition to the peak broadening, there is a shift in the position of peaks toward the lower angle side. For instance, the 2θ value of most intense peak i.e. peak corresponding to (101) plane was shifted from 36.40° to 36.25° with increase of silica concentration. The shift in the 2θ values occurred due to the increase of local strain around the impurity or lattice defects [24]. But in this case, there is a gradual shift toward the lower angle side with an increase of silica content. The shift toward lower 2θ value implies an increase in the d-spacing, indicating the presence of tensile stress acting on the ZnO nanoparticles. So, it is assumed that shift could be due to the strain introduced on ZnO nanoparticles by silica network formed around them. To confirm this, the strain and average crystallite sizes were calculated using Williamson-Hall analysis by simplified integral breadth method for ZnO and silica coated ZnO [25].

$$\beta* = \frac{1}{D} + 2\varepsilon s \quad (\text{in } \sin\theta \text{ scale})$$

where D is the average particle diameter, ε is the strain, $\beta^* = \beta\cos\theta/\lambda$, and $s = 2\sin\theta/\lambda$. The average particle diameters were obtained from this analysis. There is a gradual increase in the strain with increase in the silica content. The strain values of pristine ZnO and ZS3 based on Williamson-Hall analysis respectively are 5.29×10^{-4} and 1.94×10^{-3}. The increase in strain with increase of silica content confirmed that the shift in the peaks toward lower 2θ values is due to the strain experienced by ZnO nanoparticles.

3.2. FE-SEM and TEM analysis

Fig. 2 depicts the FE-SEM pictures of pristine ZnO and ZnO nanoparticles capped with SiO_2. These pictures demonstrate that the microstructure of ZnO nanoparticles is composed of polyhedral shaped grains. The grain size of the sample was obtained using standard deviation by counting sufficiently large number of grains to ensure accuracy. The average grain size of the pristine ZnO is 58 nm with standard deviation of 12.10 nm. The size of the ZnO nanoparticles decreased from 58 nm to 11 nm and uniform size was also attained with SiO_2 capping. No considerable change in the particle size between ZS2, ZS3 and ZS4 was found. These results are corroborated with grain size values calculated from XRD data. Fig. 3 shows the HR-TEM results of ZnO and SiO_2 capped ZnO (ZS2) nanoparticles. The particle size values obtained for ZnO and ZS2 from the pictures are 47.5 nm and 5 nm, respectively. The particle size values calculated from HR-TEM is smaller than the size calculated form XRD and FE-SEM results. Fig. 3(b) indicates that the particle size reduced with SiO_2 capping. So, it is evident from these observations that SiO_2 matrix completely covered the ZnO nanoparticles rather than forming a shell around them.

3.3. Optical absorption measurements

The UV–vis absorption spectra of ZnO, ZS1, ZS2 and ZS3 were recorded by dispersing them in ethanol, are as shown in Fig. 4. The absorption peak for pristine ZnO is positioned at 377 nm and originated from the fundamental absorption of excitons. The absorption band for bulk ZnO was previously observed at 387 nm [3]. A 10 nm shift in the absorption peak of ZnO nanoparticles toward higher energy side can be attributed to the quantum confinement effects or size effects. Further a blue shift of 10 nm was exhibited by the absorption spectra of ZS2, ZS3 and ZS4. It was shown from the FE-SEM and HR-TEM analysis that there is a decrease in particle size for the SiO_2 capped ZnO nanoparticles. So, this shift can be attributed to the decrease in the particle size of ZnO. Moreover, there is no significant shift in the absorption peak of SiO_2 capped ZnO with increase in silica content. Here, only the absorption spectra of pristine ZnO, ZS1, ZS2 and ZS3 are presented because the absorption spectrum of ZS4 was found to be the same as for ZS2 and ZS3. As can be seen from Fig. 4, as the silica concentration is increased the broadening of the absorption peaks is also increased. This kind of broadening is not observed by other investigators so far for SiO_2 capped ZnO nanoparticles. However, an increase in the peak width with increase in the shell thickness has been observed in Au nanoparticles capped with TiO_2 and ZrO_2 [26]. The increase in width is due to the confinement of free electrons within the metal core but it is true only in the case of small particles. So, the broadening of the absorption spectrum of ZS1 can be attributed to the confinement of free electrons. But in the case of samples ZS2, ZS3 and ZS4, in addition to the confinement of electrons, some other phenomena must be responsible for this kind of huge broadening. Obviously, SiO_2 matrix contributed to the new absorption peaks in ZnO–SiO_2 nanocomposites. In general, SiO_2 nanoparticles show at least two absorption peaks one at 225 nm and another at 275 nm originating from E' center and non-bridging oxygen hole centers (NBOHC) [27,28]. Recently Nonstrend et al. observed the absorption band of NBOHC along with the absorption band of ZnO nanoparticles when ZnO nanoparticles were decorated with SiO_2 [29]. So the broadening of the absorption spectra of ZS2, ZS3 and ZS4 can be attributed to the absorption of intrinsic oxygen hole centers i.e. to NBOHC in SiO_2. So, the absorption spectra are composed of absorptions due to ZnO nanoparticles as well as NBOHC in SiO_2.

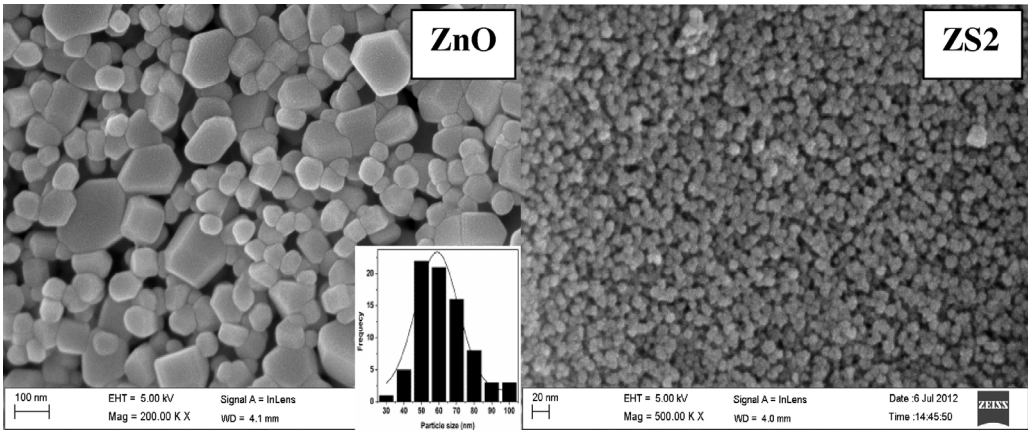

Fig. 2. FE-SEM micrographs of (a) ZnO and (b) ZS2. The inset of Fig. 2(a) shows the particle size distribution histogram of ZnO nanoparticles.

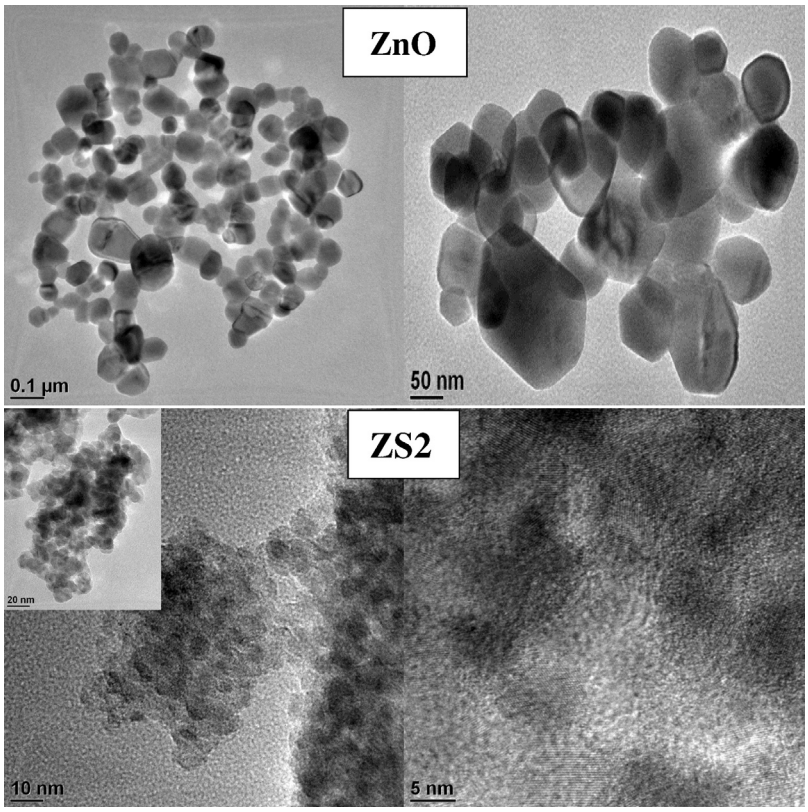

Fig. 3. HR-TEM pictures of (a) ZnO nanoparticle and (b) ZnO nanoparticles capped with SiO_2 (ZS2).

3.4. Surface properties

The surface properties of the samples were measured by the BET surface area and pore size analyzer and Zeta potential analyzer. Table 1 shows the surface area and zeta potential values for the pristine ZnO, ZS1, ZS2, ZS3 and ZS4. The surface area increased monotonously as the silica concentration increased. The surface area changed drastically from ZS1 to ZS2. It indicates that SiO_2 capping significantly changed the properties when its concentration was maintained at 0.15 (ZS2). Further increase in the concentration of SiO_2 contributed to the enhancement in the surface area. It can be understood that in the case of ZS1, a very thin layer of SiO_2 would be formed over the surface of ZnO nanoparticles for 0.05 concentrations. The high surface area of SiO_2 capped ZnO nanoparticles indicates the porous nature of the samples. The zeta potential values of ZnO and SiO_2 capped ZnO nanoparticles are shown in Table 1. The zeta potential is negative for all the samples and SiO_2 capped ZnO nanoparticles had greater zeta potential than that of the pure ZnO. The zeta potential of SiO_2 capped ZnO a nanoparticle is the same as that of the zeta potential of bare SiO_2. Since all the capped particles have higher surface charges than the uncapped ZnO particles, it is reasonable to believe that the capping agents attached to the ZnO surface [4].

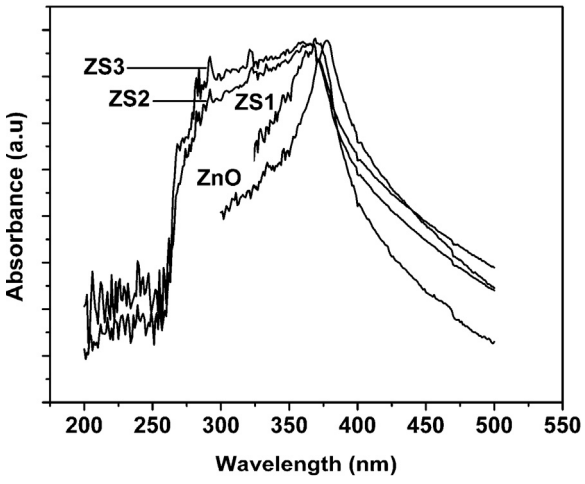

Fig. 4. UV–vis absorption spectra of ZnO (a), ZS1 (b) and ZS2 (c), ZS3 (d).

3.5. FT-IR and Raman spectroscopy

FT-IR analysis was employed to study the surface chemical structure of the samples and the results are shown in Fig. 5. FT-IR spectrum of ZnO nanoparticles showed vibrational bands at 514 cm^{-1}, 1439 cm^{-1}, 1553 cm^{-1}, 1634 cm^{-1} and 3440 cm^{-1}. The sharp peak positioned at 514 cm^{-1} is attributed to the Zn–O stretching bonds [17]. Remaining peaks are due to the O–H stretching vibrations and bending modes of adsorbed water. Two new peaks positioned at 1095 cm^{-1} and 962 cm^{-1} were observed in the IR spectrum of ZS1. These peaks can be assigned to asymmetric stretching modes of Si–O–Si vibrations and stretching modes of surface silanol groups (≡Si–OH) [30]. Thus it can be confirmed that ZnO nanoparticles were successfully capped with

Table 1
The surface area and zeta potential values of the samples.

Sample name	BET surface area (g/cm^2)	Zeta potential (mV)
ZnO	4.48	−2.72
ZS1	15.37	−24.1
ZS2	103.15	−20.9
ZS3	130.58	−20.4
ZS4	157.87	−18.9

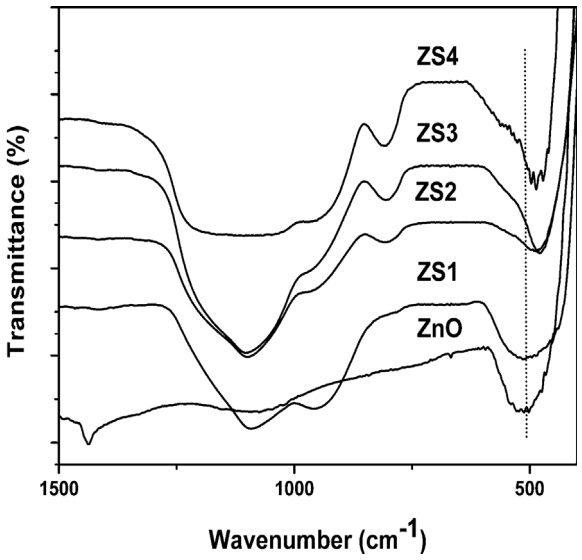

Fig. 5. FT-IR spectra of ZnO nanoparticles and ZnO nanoparticles capped with SiO_2.

SiO_2. But in ZS2, ZS3 and ZS4 the peak (514 cm^{-1}) corresponding to Zn–O stretching bonds disappeared and another peak at around 479 cm^{-1} appeared. This peak is close to the 464 cm^{-1} peak which corresponds to the bending vibrations of Si–O–Si [31]. Further, there is an enhancement in the intensity of this peak with increase in silica concentration. The increase in the intensity of 479 cm^{-1} peak with increase in silica concentration confirmed that this peak is due to the Si–O–Si bonds. The disappearance of 514 cm^{-1} peak which belongs to stretching modes of Zn–O makes it apparent that the band between 450 and 630 cm^{-1} in ZS2, ZS3 and ZS4 originated from both stretching modes of Zn–O and bend vibration modes of Si–O–Si. Moreover, the disappearance of the 962 cm^{-1} band indicates the formation of Si–O–Zn bonds [30,32]. Another peak at 803 cm^{-1} has also been observed. It is assigned to Si–O–Si stretching vibrations. It can be seen from Fig. 5 that the intensity of this peak is enhanced with increase in silica concentration suggesting that there is an improvement in the Si–O–Si stretching vibrations with increase in silica concentration.

Fig. 6 shows the micro Raman spectra of pristine ZnO and ZS1 samples. The broad peak at 330 cm^{-1} is assigned to the second-order Raman process [33]. ZnO nanoparticles are exhibiting a sharp peak at 436.8 cm^{-1}. This sharp peak is due to the $E_2^{(2)}$ phonon mode of ZnO nanoparticles. But the $E_2^{(2)}$ phonon frequency of the bulk ZnO substrate is located at 438.5 cm^{-1}. Yang et al. also observed a blue shift of nearly 2 cm^{-1} compared to the bulk ZnO $E_2^{(2)}$ phonon frequency [33]. This blue shift was previously attributed to the optical phonon confinement effects [34] or the presence of intrinsic defects on the nanoparticles [35]. The intensity of this peak is greatly reduced in ZS1. This is due to the fact that ZnO nanoparticles are surrounded by the SiO_2 matrix which is generally insensitive to the Raman spectroscopy [36]. A weak intense peak at 438.5 cm^{-1} was detected in the Raman spectrum of ZS1. With silica encapsulation, the peak again shifted to bulk ZnO position. It is known that the surface defects of nanoparticles can be reduced significantly by the passivation of their surfaces with materials of high dielectric constant. The passivation of surfaces contributes to the enhancement of UV and visible emission intensities. The improvement in the UV emission with the increase of silica content can be seen in PL results discussed in the following section. By combining (i) enhancement in the UV emission and (ii) shift of ZnO $E_2^{(2)}$ phonon frequency from bulk ZnO position, it can be concluded that blue shift of 2 cm^{-1} shown by ZnO nanoparticles is due to the presence of defects on the nanoparticles. Another peak positioned at 583 cm^{-1} belongs to E_1 phonon, which indicates that c-axis of wurtzite ZnO is perpendicular to the particle surface.

3.6. Photoluminescence analysis

Fig. 7 shows the PL spectra of ZnO, ZS1, ZS2, ZS3 and ZS4. The sharp peak which is shifted with excitation wavelength is due to the sample holder [37]. Gaussian fitting has been used to know the exact number and position of peaks. The PL of ZnO is composed of four emission peaks positioned at 398 nm, 434 nm, 466 nm and 492 nm. Most familiar green emission of ZnO could not be observed in these samples. Among these four emission peaks, one at 398 nm originated from the electron transition from the localized level slightly below conduction band to the valence band [38,45]. The emission peak at 434 nm has been attributed previously to the electron transition from defect level created by zinc interstitial to the top of the valence band [39,40]. Another emission at 466 nm is assigned to intrinsic defects such as oxygen and zinc interstitials [40,41]. Finally, a weak emission peak at 492 nm in these samples can be assigned to various deep level defect states originating from the zinc interstitials and/or oxygen vacancies [41]. Even though there are many reports on visible luminescence of ZnO, its origin is still controversial. This is due to the variety of synthesis procedures that have been used to prepare

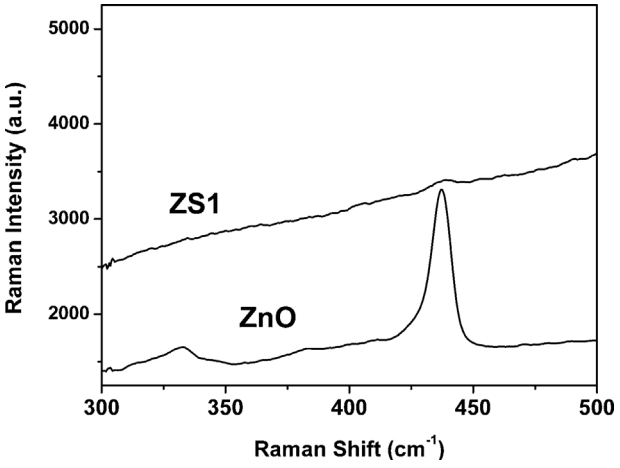

Fig. 6. Raman spectra of pristine ZnO and ZS1.

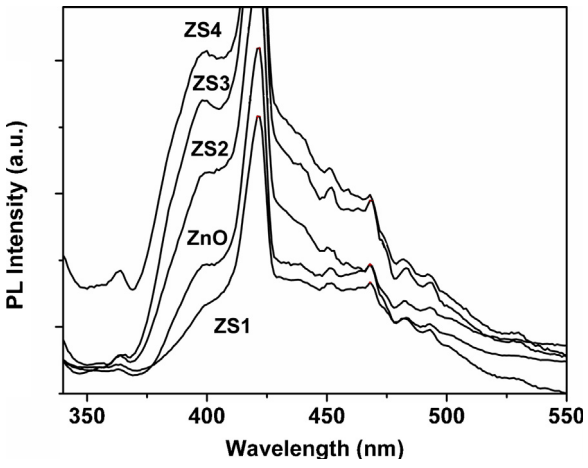

Fig. 7. PL spectra of ZnO nanoparticles and ZnO nanoparticles capped with SiO_2 recorded with an excitation wavelength of 320 nm.

ZnO nanoparticles and also due to complexity in its microstructure. Fig. 7 shows that there is a monotonous increase in UV emission intensity with increase of silica concentrations except in ZS1. The decrease in the emission intensity of ZS1 can be explained as follows: As the particle size decreases, surface area to volume ratio increases which gives rise to larger non-radiative relaxation paths. With large non-radiative relaxation path, the passivation of ZnO nanocrystals does not necessarily lead to the enhancement of the NBE, because the excess energy saved by the passivation is consumed by the non-radiative relaxation path [11,42]. Wu et al. observed that the UV and yellow-green emission intensities increase with increase of shell thickness of SiO_2 [4]. Very recently, Cao et al. also found that there is an increase in UV and visible emission intensities of ZnS:Mn^{2+}/ZnO with SiO_2 passivation [22]. In the case of ZnO nanoparticles, surface states such as dangling bonds contribute to the non-radiative processes. The enhancement in the UV emission intensity might be due to the reduction of dangling bonds of ZnO with SiO_2 capping. It was confirmed from the XRD analysis that strain is acting on the ZnO nanoparticles as the silica concentration is increased. In the case of core shell nanoparticles, localized strain and interface effects also had an influence on optical properties [43,44]. This induced strain causes the shift in the position of emission peaks. But, in this study such shifts were not observed and hence UV emission at 398 nm is independent of strain. It was found that optimum UV emission intensity can be obtained when the excitation wavelength is chosen from the PL excitation spectrum (PLE) [45]. So, the PLE spectra of both ZnO and silica coated ZnO (ZS4) were recorded by monitoring the emission wavelength at 390 nm and presented in Fig. 8. PLE spectrum of ZnO showed a peak at 353 nm where as ZS4 exhibited two more peaks at 275 nm and 295 nm in addition to 353 nm PLE peak. Obviously, these two peaks positioned at 275 nm and 295 nm are evolved due to the excitation processes in SiO_2. Similar peaks were also observed in the UV–vis absorption spectra of ZS2, ZS3 and ZS4. It indicates good correlation between absorption spectra and PLE spectra of these samples. So the broadening of absorption spectrum of ZS2, ZS3 and ZS4 can be assigned to absorption processes in SiO_2 along with ZnO absorption. The PLE peak at 275 nm is in good agreement with the optical absorption results and attributed to the non-bridging oxygen hole centers [29]. Generally, three types of silanol groups are covered on the porous SiO_2 surface namely single, hydrogen bonded and germinal silanol groups [46]. The NBOHC are generated from the single silanol groups which are formed after the dehydroxylation of hydrogen bonded silanol groups. The contribution of NBOHC to the enhancement of the UV emission intensity of ZnO nanoparticles can be understood as follows. The NBOHC are in positive charge state i.e. (≡Si–O•) or the net charge on the NBOHC is +ve. So they readily accept an electron from ZnO because it is generally an n-type semiconductor. This phenomenon resulted in the formation of ≡Si–O–Zn bonds on the surface of the ZnO. So the oxygen from the ambient was prevented from being attached to the ZnO surface. The formation of ≡Si–O–Zn bands and their enhancement with increase of SiO_2 concentration was confirmed from UV–vis and FT-IR results. Fu et al. results also confirmed the formation of ≡Si–O–Zn bands in ZnO–SiO_2 nanocomposites [47]. The electrons that are trapped at the NBOHC make transitions to conduction band and the level slightly below it and increase the PL intensity. As the silica concentration is increased, more number of carriers are excited in SiO_2 and hence there are more number of carriers available in the conduction band and the state which is slightly below the conduction band of ZnO. So there are more number of radiative transitions to the valence band of ZnO. Consequently, the UV emission intensity of ZnO nanoparticles increases. This mechanism is illustrated in Fig. 9. As stated above, maximum UV emission intensity can be obtained with an excitation wavelength chosen from PLE spectrum. So, the PL spectra of samples were acquired with an excitation wavelength of 353 nm and results are shown in Fig. 10. There is five times enhancement in the intensity of UV emission peak positioned at 398 nm with silica capping. In addition, there is also enhancement in the visible emission. It can be seen in ZS1 that a hump is developed at 418 nm with SiO_2 capping. This emission is generally attributed to the oxygen vacancies at the interface of ZnO [48]. The improvement in the intensities of 418 nm and 522 nm emissions indicates that ZnO–SiO_2 nanocomposite is rich in oxygen vacancies. Furthermore, another peak at 585 nm (yellow emission) is also evolved with silica coating. The yellow emission can be attributed to intrinsic defects in ZnO such as oxygen interstitials [49]. It can be confirmed that with SiO_2 coating of ZnO nanoparticles, there is enhancement in the UV emission intensity of ZnO and some new defect states were also created.

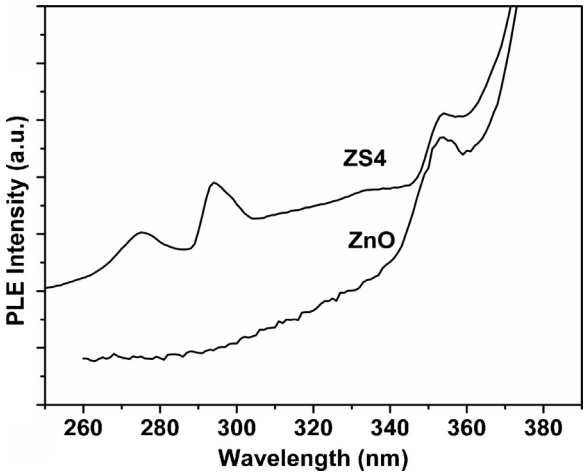

Fig. 8. Photoluminescence excitation spectra of ZnO and ZS4 recorded by monitoring the emission wavelength at 390 nm.

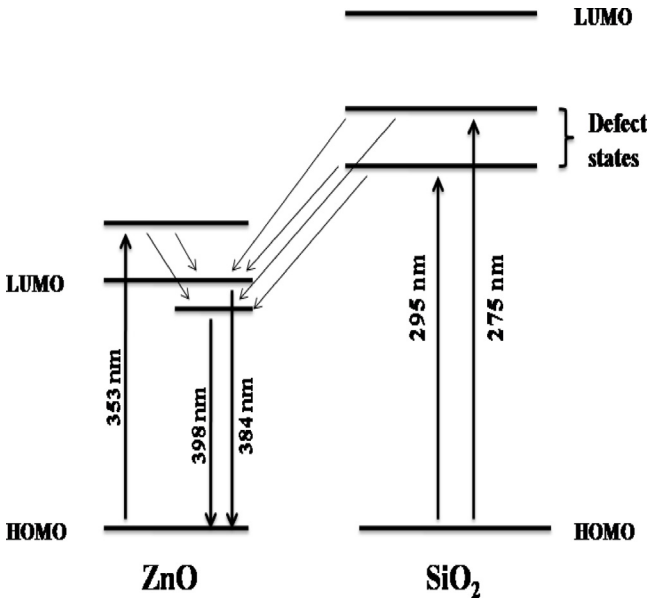

Fig. 9. Schematic representation for the excitation and emission processes responsible for the enhancement of the UV emission intensity.

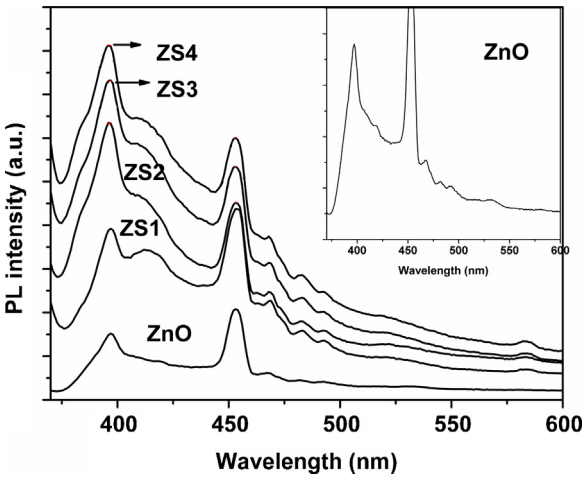

Fig. 10. PL spectra of ZnO nanoparticles and ZnO nanoparticles capped with SiO_2 recorded with an excitation wavelength of 353 nm.

4. Conclusions

The effect of SiO_2 capping on structural and optical properties of ZnO nanoparticles was investigated. Uniform and small ZnO nanoparticles were achieved with SiO_2 capping. X-ray diffraction analysis showed that at high silica concentration, ZnO nanoparticles are under strain. The reduction in particle size was reflected as blue shift in the absorption spectrum. Raman analysis of the samples indicated that the shift in the 438.5 cm^{-1} mode of ZnO is due to the surface defects. It is found that UV emission intensity was enhanced with increase of SiO_2 content in the nanocomposite. The emission spectra were measured with 320 nm excitation and 353 nm excitation wavelengths. Maximum UV emission intensity is observed with 353 nm excitation wavelength in pristine ZnO as well as in SiO_2 coated ZnO nanoparticles. The increase in the emission intensities was attributed to the surface passivation of ZnO nanoparticles and excitation process in SiO_2. Moreover, there is enrichment of oxygen vacancies and interstitials with increase of silica concentration.

Acknowledgements

The authors are thankful to Prof. K. Sethupathi, IIT Madras, Chennai, for providing HR-TEM measurements generously. Authors would like to thank Y.B. Ravi Sankar for providing XRD measurements.

References

[1] Ü. Özgür, Ya.I. Alivov, C. Liu, A. Teke, M.A. Reshchikov, S. Doğan, V. Avrutin, S.J. Cho, H. Morkoç, J. Appl. Phys. 98 (2005) 041301.
[2] N. Hagura, T. Takeuchi, S. Takayama, F. Iskandar, K. Okuyama, J. Lumin. 131 (2011) 138.
[3] P.K. Giri, S. Bhattacharyya, Dilip K. Singh, R. Kesavamoorthy, B.K. Panigrahi, K.G.M. Nair, J. Appl. Phys. 102 (2007) 093515.
[4] Y.L. Wu, C.S. Lim, S. Fu, A.I.Y. Tok, H.M. Lau, F.Y.C. Boey, X.T. Zeng, Nanotechnology 18 (2007) 215604.
[5] W.J. Huang, G.C. Fang, C.C. Wang, Colloids Surf. A 260 (2005) 45.
[6] C. Dai, B. Wang, H. Zhao, Colloids Surf. B 41 (2005) 117.
[7] B.H. Zeng, G. Duan, Y. Li, S. Yang, X. Xu, W. Cai, Adv. Fun. Mater. 20 (2010) 561.
[8] R. Dingle, Phys. ReV. Lett. 23 (11) (1969) 579.
[9] E.Z. Mollwo, Phys. 138 (1954) 478.
[10] F.A. Kröger, H.J. Vink, J. Chem. Phys. 22 (2) (1954) 250.
[11] A. Van Dijken, E.A. Meulenkamp, D. Vanmaekelbergh, A. Meijerink, J. Phys. Chem. B 104 (2000) 1715.
[12] A. Sharma, B.P. Singh, S. Dhar, A. Gondorf, M. Spasova, Surf. Sci. 606 (2012) L13.
[13] B. Yao, H. Shi, H. Bi, L. Zhang, J. Phys. Condens. Matter. 12 (2000) 6265.
[14] G.Q. Tang, Y. Xiong, L.Z. Zhang, G.L. Zhang, Chem. Phys. Lett. 395 (2004) 97.
[15] S. Panigrahi, A. Bera, D. Basak, J. Colloid Interface Sci. 353 (2011) 30.
[16] M.K. Patra, M. Manoth, V.K. Singh, G. Siddaramana Gowd, V.S. Choudhry, S.R. Vadera, N. Kumar, J. Lumin. 129 (2009) 320.
[17] C.R. Shabnam, P. Kant, Arun, Mater. Res. Bull. 45 (2010) 1368.
[18] R.G. Singh, F. Singh, D. Kanjilal, V. Agarwal, R.M. Mehra, J. Phys. D: Appl. Phys. 42 (2009) 062002.
[19] M.S. Kim, K.G. Yim, S. Kim, G. Nam, J.Y. Leem, J. Sol. Gel. Sci. Technol. 59 (2011) 364.
[20] S. Panigrahi, A. Bera, D. Basak, ACS Appl. Mater. Interfaces 1 (2009) 2408.
[21] N. Hagura, T. Takeuchi, S. Takayama, F. Iskandar, K. Okuyama, J. Lumin. 131 (2011) 921.
[22] J. Cao, J. Yang, L. Yang, M. Wei, B. Feng, D. Han, L. Fan, B. Wang, H. Fu, J. Appl. Phys. 112 (2012) 014316.
[23] B.D. Cullity, S.R. Stock, Elements of X-ray Diffraction, 3rd ed., Prentice Hall, New Jercy, 2001.
[24] X.M. Teng, H.T. Fan, S.S. Pan, C. Ye, G.H. Li, J. Phys. D: Appl. Phys. 39 (2006) 471.
[25] M. Ghosh, A.K. Raychaudhuri, J. Appl. Phys. 100 (2006) 034315.
[26] R.T. Tom, A.S. Nair, N. Singh, M. Aslam, C.L. Nagendra, R. Philip, K. Vijayamohanan, T. Pradeep, Langmuir 19 (2003) 3439.
[27] R. Weeks, C. Nelson, J. Appl. Phys. 31 (1960) 1555.
[28] L. Skuja, R. Silin, Phys. Stat. Sol. 56 (1979) 1.
[29] J.E.V. Nostrand, R. Cortez, Z.P. Rice, N.C. Cady, M. Bergkvis, Nanotechnology 21 (2010) 415602, http://dx.doi.org/10.1088/0957-4484/21/41/415602.
[30] Q. Jiang, Z. Wu, Y. Wang, Y. Cao, C. Zhou, J. Zhu, J. Mater. Chem. 16 (2006) 1536.
[31] F. Li, X. Huang, Y. Jiang, L. Liu, Z. Li, Mater. Res. Bull. 44 (2009) 437–441.
[32] Y. Xiong, L.Z. Zhang, G.Q. Tang, G.L. Zhang, W.J. Chen, J. Lumin. 110 (2004) 17.
[33] R.D. Yang, S. Tripathy, Y. Li, H.J. Sue, Chem. Phys. Lett. 411 (2005) 150.
[34] M. Rajalakshmi, A.K. Arora, B.S. Bendre, S. Mahamuni, J. Appl. Phys. 87 (2000) 2445.
[35] K.A. Alim, V.A. Fonoberov, A.A. Balandin, Appl. Phys. Lett. 86 (2005) 053013.
[36] J. Liu, J. Niu, D. Yang, M. Yan, J. Sha, Physica E 23 (2004) 221.
[37] K. Sowri Babu, A. Ramachandra Reddy, Ch. Sujatha, K. Venugopal Reddy, Ceramint 39 (2012) 3055–3064.
[38] X.D. Gao, X.M. Li, W.D. Yu, Appl. Surf. Sci. 229 (2004) 275–281.
[39] X.P. Peng, H. Zang, Z.G. Wang, J.Z. Xu, Y.Y. Wang, J. Lumin. 128 (2008) 328.
[40] B.D. Ngom, O. Sakho, N. Manyala, J.B. Kana, N. Mlungisi, L. Guerbous, A.Y. Fasasi, M. Maaza, A.C. Beye, Appl. Surf. Sci. 255 (2009) 7314.
[41] A.K. Singh, V. Viswanath, V.C. Janu, J. Lumin. 129 (2009) 874.
[42] S. Yamamoto, T. Mishina, J. Lumin. 131 (2011) 620.
[43] Y.M. Niquet, G. Allan, C. Delerue, M. Lannoo, Appl. Phys. Lett. 77 (2000) 1182.
[44] M.S. Sander, R. Gronsky, Y.M. Lin, M.S. Dresselhaus, J. Appl. Phys. 89 (2001) 2733.
[45] K. Sowri Babu, A. Ramachandra Reddy, Ch. Sujatha, K. Venugopal Reddy, Mater. Lett. 99 (2013) 97.
[46] J.L. Shen, C.F. Cheng, Curr. Opin. Solid State Mater. Sci. 7 (2003) 427–433.
[47] Z. Fu, B. Yang, L. Li, W. Dong, C. Jia, W. Wu, J. Phys. Condens. Matter. 15 (2003) 2867–2873.
[48] B.J. Jin, S. Im, S.Y. Lee, Thin Solid Films 366 (2000) 107–110.
[49] L. Wu, Y. Wu, Y. Lu, Mater. Res. Bull. 41 (2006) 128–133.